UNIVERSIDADE ESTADUAL PAULISTA
"JÚLIO DE MESQUITA FILHO"
Câmpus de São José do Rio Preto

Ag/NiO nanocomposites derived from α-nickel hydroxide for the detection of microbial volatile organic compounds

Gabriel Camilo Negrini Vioto

São José do Rio Preto

2021

Gabriel Camilo Negrini Vioto

Ag/NiO nanocomposites derived from α-nickel hydroxide for the detection of microbial volatile organic compounds

Dissertação apresentada como parte dos requisitos para obtenção do título de Mestre em Química, junto ao Programa de Pós-Graduação em Química, do Instituto de Biociências, Letras e Ciências Exatas da Universidade Estadual Paulista "Júlio de Mesquita Filho", Campus de São José do Rio Preto.

Financiadora: CAPES – Proc. 88882.434462/2019-01

Orientador: Prof. Dr. Diogo Paschoalini Volanti

São José do Rio Preto
2021

V799a

Vioto, Gabriel Camilo Negrini

Ag/NiO nanocomposites derived from alpha-nickel hydroxide for the detection of microbial volatile organic compounds / Gabriel Camilo Negrini Vioto. -- São José do Rio Preto, 2021

42 f. : il., tabs.

Dissertação (mestrado) - Universidade Estadual Paulista (Unesp), Instituto de Biociências Letras e Ciências Exatas, São José do Rio Preto

Orientador: Diogo Paschoalini Volanti

1. Química inorgânica. 2. Compostos orgânicos voláteis microbianos. 3. Óxido de níquel. 4. Nanocompósito. I. Título.

Sistema de geração automática de fichas catalográficas da Unesp. Biblioteca do Instituto de Biociências Letras e Ciências Exatas, São José do Rio Preto. Dados fornecidos pelo autor(a).

Essa ficha não pode ser modificada.

Gabriel Camilo Negrini Vioto

Ag/NiO nanocomposites derived from α-nickel hydroxide for the detection of microbial volatile organic compounds

Dissertação apresentada como parte dos requisitos para obtenção do título de Mestre em Química, junto ao Programa de Pós-Graduação em Química, do Instituto de Biociências, Letras e Ciências Exatas da Universidade Estadual Paulista "Júlio de Mesquita Filho", Campus de São José do Rio Preto.

Financiadora: CAPES – Proc. 88882.434462/2019-01

Comissão Examinadora

Prof. Dr. Diogo Paschoalini Volanti
UNESP – São José do Rio Preto
Orientador

Prof. Dr. Márcio José Tiera
UNESP – São José do Rio Preto

Prof. Dr. Waldir Avansi Junior
UFSCar – São Carlos

São José do Rio Preto
10 de Junho de 2021

ACKNOWLEDGMENTS

First, I thank my family for all the support, care, and instruction during challenging times. In particular, my parents, Ana Lúcia and Eduardo, went out of their way to support me in all possible ways for all the opportunities they gave me. My girlfriend Laura, for the conversations and companionship, always keeping me in any situation. I am grateful to my advisor, Diogo, for the opportunities, confidence, and discussions contributing to my academic training and personal development. I acknowledge all my laboratory companions at LabMatSus for their friendship, especially Tarcísio and Cecilia, for their help and dedication to my academic development. I thank CAPES for the master's scholarship granted. Finally, I would like to thank the LSQA/IBILCE-UNESP for carrying out the techniques of XRD, FTIR, and LMA/IQ-UNESP by the analysis of FESEM. This study was financed in part by the Coordenação de Aperfeiçoamento de Pessoal de Nível Superior - Brasil (CAPES) - Finance Code 001.

ABSTRACT

Microorganisms are widely studied due to the risks they can cause in human activities. It can damage the economy and health fields, causing infectious diseases or even the deterioration of food. Thus, there is a need for the control and identification of these organisms. An essential characteristic of microorganisms, in general, is that they produce specific profiles of microbial volatile organic compounds (mVOC) in their cellular metabolism, which can be correlated with infectious diseases or even particular microorganisms. In this work, α-nickel hydroxide (α-$Ni(OH)_2$) and silver (Ag) were used as a precursor of nickel oxide (NiO) and for decorating NiO with different amounts of % mass, respectively. They aim to obtain materials (NiO and Ag/NiO) with pores and silver in their structures. The modifications can guarantee better performance in applying the material both as a sensor for mVOCs and VOCs, through sensitization reactions, caused by the presence of Ag. For selectivity of the samples, acetone, ethanol, 2-butanone, 3-methyl-1-butanol, 2-nonanone, and m-xylene were used; a better selectivity was obtained for 3-methyl-1-butanol, a mVOC. In addition, sensitivity tests were performed, using different concentrations of 3-methyl-1-butanol in a range of 2 to 200 ppm and a test to obtain the optimum operating temperature of the materials.

Keywords: Microbial volatile organic compounds. α-Nickel hydroxide. N**ickel oxide. Silver decorating. Nanocomposite.**

RESUMO

Os micro-organismos são amplamente estudados devido aos riscos que podem ocasionar nas atividades humanas. Podendo causar danos desde a área da saúde até a área econômica, ocasionando doenças infecciosas ou mesmo a deterioração de alimentos. Dessa forma, surge a necessidade do controle e identificação destes organismos. Uma importante característica dos micro-organismos em geral é que estes produzem perfis específicos de compostos orgânicos voláteis (mCOVs) em seu metabolismo celular, perfis estes que podem ser correlacionados com doenças infecciosas ou mesmo micro-organismos específicos. Neste trabalho, foi utilizado de α-hidróxido de níquel, como precursor para síntese de óxido de níquel (NiO) e do NiO decorado com diferentes quantidades de % massa de Ag, respectivamente. Visando a obtenção de materiais (NiO e Ag/NiO) com morfologias semelhante a pétalas e com prata em suas estruturas. Modificações estas que podem promover um melhor desempenho na aplicação do material tanto como sensor de mCOVs quanto de COVs, possivelmente obtida por reações de sensibilização, ocasionadas pela presença de Ag. Em seguida, foram realizados testes de seletividade para as amostras. Para a seletividade foram utilizados, acetona, etanol, 2-butanona, 3-metil-1-butanol, 2-nonanona e m-xileno, onde foi obtido uma melhor seletividade para o 3-metil-1butanol, um exemplo de mCOV. Além disso, foram realizados testes de sensibilidade, utilizando diferentes concentrações de 3-metil-1-butanol em uma faixa de 2 a 200 ppm. Também foram realziados testes para a obtenção da temperatura de trabalho das amostras.

Palavras-chave: Compostos orgânicos voláteis microbianos. α-Hidróxido de níquel. Óxido de níquel. NiO decorado com Ag. Nanocompósitos.

LISTA DE ILUSTRAÇÕES

Figure 1 - a,b) Papers of n-type and p-type oxide semiconductor gas sensors reported in the literature. c,d) Formation of electronic core-shell structures in n-type and p-type metal oxide semiconductors. ……..…….13

Figure 2 - Sensitization mechanism. a) Electronic sensitization b) chemical sensitization. ……...14

Figure 3 - Schematic illustration of the VOC-sensing measurement setup. a) air cylinder; b) flow meter; c) VOC injection syringe; d) septum to insert the VOC; e) tubular oven; f) interdigital alumina electrode containing deposited sample; g) thermocouple; h) PID temperature controller; i) Keithley Source Measure Unit, and j) visualization of the resistance variation with time. ……23

Figure 4 - XRD patterns of α-$Ni(OH)_2$. ……24

Figure 5 - XRD patterns of NiO. ……...25

Figure 6 - a) XRD patterns of 0.5% Ag/NiO and 1% Ag/NiO. b) XRD patterns of 2% Ag/NiO and 5% Ag/NiO. ……...26

Figure 7 - FESEM images (a,b,c) *α-$Ni(OH)_2$* and (d,e,f) NiO with different magnifications. ……...27

Figure 8 - FESEM images a,b) 0.5% Ag/NiO; c,d) 1% Ag/NiO; e,f) 2% Ag/NiO; 5% Ag/NiO, with different magnifications. ……..28

Figure 9 - a) EDX spectrum of NiO and b) 5% Ag/NiO. ...……...29

Figure 10 - FTIR spectra of NiO; 0.5% Ag/NiO ; 1% Ag/NiO; 2% Ag/NiO and 5% Ag/NiO. ……..30

Figure 11 - (a) Survey XPS spectra of the sample. High-resolution XPS spectra of (b) O 1s, (c) Ni 2p, and (d) Ag 3d. ……...31

Figure 12 - a) Response to 100 ppm 3-methyl-1-butanol of NiO at different operating temperatures (200-350°C), b) response to 100 ppm of different VOCs and mVOCs at the optimum operating temperatures (250 °C), c) resistance changes of NiO upon exposure to 3-methyl-1-butanol in the concentration range of 5-200 ppm, d) response of NiO to 3-methyl-1-butanol in a concentration range of 5-200 ppm. ……..32

Figure 13 - Response to 100 ppm 3-methyl-1-butanol of NiO with different percentages of silver. ……..33

Figure 14 - a) Response to 100 ppm 3-methyl-1-butanol of Ag/NiO 5% at different operating temperatures (200-350°C), b) response to 100 ppm of different VOCs and mVOCs at the optimum operating temperatures (200 °C), c) resistance changes of Ag/NiO 5% upon exposure to 3-methyl-1-butanol in a concentration range of 5-200 ppm, d) response of Ag/NiO 5% to 3-methyl-1-butanol in a concentration range of 5-200 ppm. ……34
Figure 15 - Figure 15. Responses of NiO and Ag/NiO 5% as a function of 3-methyl-1-butanol concentration at a related optimum operating temperature under a wet atmosphere of 56%. 35

LISTA DE TABELAS

Table 1 - Crystallite size and crystallinity of the samples. ……26
Table S1 - Ag/NiO 0.5% response to six different VOCs. ……41
Table S2 - Ag/NiO 1% response to six different VOCs. ……...41
Table S3 - Ag/NiO 2% response to six different VOCs. ……...41
Table S4 - Ag/NiO 5% response to six different VOCs. ……...42

LISTA DE ABREVIATURAS E SIGLAS

VOC	Volatile organic compound
mVOC	Microbial volatile organic compound
LMs	*Listeria Monocytogenes*
MVP	Mechanically ventilated patients
CG-MS	Gas chromatography coupled to a mass spectrometer
SMO	Semiconductor metal oxide
HAL	Hole accumulation layer
TEFLON	Polytetrafluoroethylene
XRD	X-ray diffraction
FTIR	Fourier transform infrared
FESEM	Field-emission scanning electron microscopy
EDX	Energy-dispersive X-ray spectroscopy
XPS	X-ray photoelectron spectroscopy
FWHM	Full width at half-maximum
RH	Relative humidity
2D	Two-dimensional

SUMMARY

1 General introduction and aim of this work…….11

2 Effect of Ag on NiO derived from α-nickel hydroxide structures obtained by microwave-assisted solvothermal method for the detection of 3-methyl-1-butanol……19

2.1 Introduction……...20

2.2 Experimental section…….……21

2.2.1 Preparation of NiO from α-$Ni(OH)_2$……....21

2.2.2 Ag/NiO preparation…….21

2.2.3 Characterization……...21

2.2.4 VOCs-sensing measurements……..22

2.3 Results and discussion……...23

2.4 Conclusion……..35

3 General Conclusions……..40

APÊNDICE A – Response of Ag/NiO samples to six different to six different VOCs.……...……...…41

1 General introduction and aim of this work

Volatile organic compounds (VOCs) are compounds that have high vapor pressure, which facilitates their boiling at low temperatures (ex: 50 ° C to 260 ° C)[1]. Contact with VOCs can adversely affect human health, short-term or long-term health effects[2]. As the risk of exposure to VOCs increases, strict environmental regulations and indoor air quality[3].

VOCs can also be used as disease biomarkers. They can be generated in the human body due to changes in metabolic pathways and be emitted in body fluids such as breathing, urine, saliva, and blood[4,5]. The same goes for the cellular metabolism of all living organisms, such as fungi, mold, and bacteria, which can produce a wide variety of extracellular metabolites, some of which are volatile (mVOCs)[6–8]

Microorganisms present in the environment represent a risk for many human activities[9], such as food spoilage[7], pathogenicity[8,10,11]. As a result of the different metabolisms they present, various pathogens produce specific profiles of mVOCs. The analysis of these particular profiles allows the correlation of mVOC with indicative of specific diseases and infections. One of the most critical contamination routes by microorganisms occurs through ingestion, whether accidental or intentional, exposure to contaminated drinking water, wastewater, soil, and food sources[12]. In the last decades, many countries have documented a significant increase in the incidence of diseases caused by microorganisms' presence in food. Contamination of food by microbiological agents is a worldwide public health concern[7].

Some examples related to food spoilage are grains and oilseeds that generate mycotoxins that can cause chronic health problems to humans and animals when stored during an extended period. The detection of specific mVOCs made it possible to use an mVOC sensor to indicate fungal growth[6]. For example, several diseases are related to microorganisms; *Listeria Monocytogenes* (LMs) is a pathogenic microbe present in food, responsible for bacteremia, meningitis, and complications during pregnancy. It grows in foods such as meats, vegetables, seafood, and even in domestic refrigerators. In the case of LMs, the main exhaled volatile organic compound (VOC) is 3-hydroxy-2-butanone[13] and 2-nitrophenol[14] and can be used as a biomarker for indirect detection of this microorganism.

Among infectious lung diseases, pneumonia is the second most common cause of death, second only to lung cancer. Nosocomial pneumonia is also the second most

common cause of nosocomial infections after urinary tract infection[15]. Nosocomial pneumonia complications are associated with mechanically ventilated patients (MVP). The mortality rate for MVP can be relatively high, ranging from 24 to 76%. MVP can be caused by pathogens, such as *Staphylococcus aureus* and *Pseudomonas aeruginosa*[15]; these microorganisms can be identified through the detection of some VOCs, such as acetoin[16], isovaleric acid[16], acetic acid[14,16], and 3-methyl-1-butanol[15] for *Staphylococcus aureus* and 2-nonanone[16,17] and 3-methyl-1-butanol[15] for *Pseudomonas aeruginosa*. Therefore, sensors' application to detect metabolites derived from pathogens, especially in mechanically ventilated patients, is entirely feasible. It is not invasive, and the results are available immediately after the measurement. Due to these concerns, there was an increase in sensor technologies in hospitals, industries, and agriculture[9].

Conventional methods for identifying VOCs and microorganisms are gas chromatography coupled to a mass spectrometer (CG-MS)[8,10,11,18] and cultivation and biochemical tests[6], respectively. However, they become unfeasible because they are expensive, robust[5,11], complicated, and time-consuming[19] techniques. An alternative widely studied to these problems is the development of semiconducting metal oxides (SMOs) for application in detecting VOCs; the interest arises due to the high sensitivity, selectivity, portability, and low cost[5,20–23] that the material can present.

Chemiresistive sensors use a reaction mechanism (oxidation) of the studied mVOCs due to the presence of oxygen species adsorbed on the material surface, which causes a depletion layer (n-type semiconductors) or a layer of accumulation of holes (p-type semiconductors)[24]. As shown in Figure 1c,d, the VOCs detection mechanism occurs through reactions present on the sensor surface. In p-type SMO, when the material is exposed to air, molecular oxygen adsorbs on the material's surface, thus removing electrons—generating ionized oxygen species on its surface and a hole accumulation layer (HAL) the electrons used in the ionosorption. The ionosorbed oxygen species on the surface react with the specific VOC, oxidizing it to CO_2 and H_2O[21,24]. In this way, the electrons previously captured recombine with the holes, thus promoting resistance increasing. When the material is exposed to atmospheric air again, oxygen species will adsorb on the material's surface, forming the HAL, changing the resistance again.

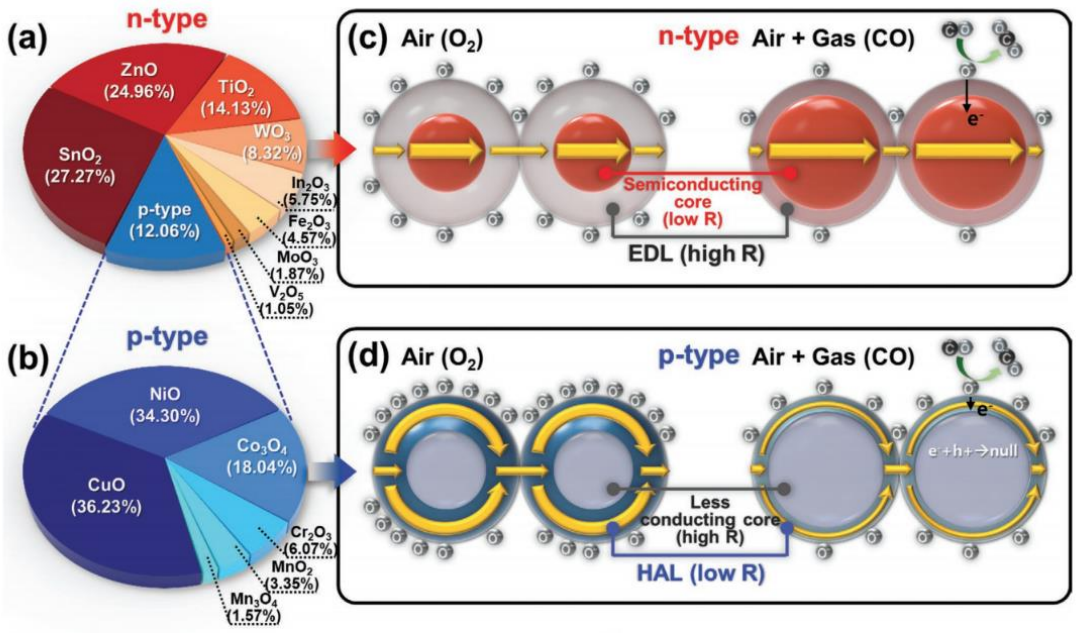

Figure 1. a,b) Papers of n-type and p-type oxide semiconductor gas sensors reported in the literature. c,d) Formation of electronic core-shell structures in n-type and p-type metal oxide semiconductors. **Reference:** JEONG, KIM, LEE, 2020[24].

P-type SMOs usually have an inadequate response as a sensor than n-type SMOs, making it difficult to commercialize. Despite the smaller number of studies related to p-type sensors as presented in Figure 1a,b, an area of active research appears to increase the performance of these sensors. The application of p-type SMO should not be underestimated and overlooked, as most p-type semiconductors are widely used as valuable catalysts. The choice of metal oxide and characteristics such as surface area, and morphology can directly affect the sensor's performance [24].

NiO is widely studied for applications such as electrochromic [25], supercapacitor [26], and battery systems [27]. In addition, it was presenting high physical stability and good electrical properties[28], making it an exciting material for gas sensing. Besides, several alternatives can be explored to improve the performance of SMOs as a sensor, including the use of methodologies for morphology control and functionalization methods with noble metals, aiming at increasing the material's contact surface and sensitization reactions, respectively.

α-$Ni(OH)_2$ has a hydroxyl-deficient, thus positively charged, with a structure similar to hydrotalcite. The interlayer distance is approximately 7 Å, more significant than that presented by its polymorphs. α-$Ni(OH)_2$ contains intercalated anions and water molecules in its interlamellar spacing; their layers are oriented randomly, giving a

greater degree of disorder. The large interlamellar distance directly influences the characteristics of α-$Ni(OH)_2$, resulting in interlayer chemistry and electrochemical activity. Thus, presenting electrochemical features superior to β-$Ni(OH)_2$, in addition to being a material that can be easily transformed into a p-type semiconductor. However, α-$Ni(OH)_2$ is unstable and difficult to prepare, as this phase may change rapidly to beta form during synthesis or storage[29,30].

Also, noble metals such as Ag, Pd, Au, and Pt can cause SMO synergistic effects, thus improving the material's performance in the application as a gas sensor. These synergistic effects can occur in two main ways, through electronic and chemical sensitization reactions. In electronic sensitization, Figure 2a, the metal in its oxidized state removes electrons from the SMO, inducing the formation of an electron-depleted space-charge layer close to the surface between the metal and the SMO. Thus, reducing the layer of hole accumulations and changing the resistance. When the material is exposed to analytic gas, the metal is reduced, and the electrons return to the SMO. Chemical sensitization, Figure 2b, occurs through the spill-over effect, resulting from a catalytic surface reaction. The deposited metal activates the analyzed gas molecules, facilitating their subsequent reaction with ionosorbed oxygen on the sensor surface. In this situation, the metal does not affect the sensor's resistance and can cause an increase in sensitivity, increasing the reaction rate of chemical processes[31-33].

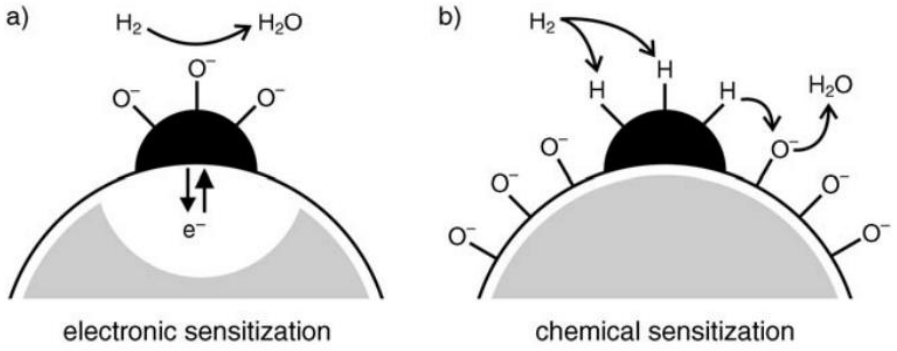

Figure 2. Sensitization mechanism. a) Electronic sensitization b) chemical sensitization.
Reference: FRANKE; KOPLIN; SIMON, 2006.

Therefore, this dissertation aims to explore Ag decorated NiO (p-type semiconductor), derived from α-$Ni(OH)_2$ to detect mVOCs. The overall structure of the dissertation takes the form of three chapters, including the present chapter. Chapter 2 provides new insights into the methodologies for the synthesis of NiO and Ag/NiO, which will be given for carrying out VOCs-sensing tests, the characterization of

materials, in addition to VOCs-sensing properties for NiO and Ag/NiO 5%. Finally, chapter three presents the general conclusion of the dissertation.

References

[1] C. Baird, M. Cann, Environmental Chemistry, W. H. Free, W. H. Freeman and Company, New Work, 2012.

[2] V. Soni, P. Singh, V. Shree, V. Goel, Effects of VOCs on Human Health, in: 2018: pp. 119–142. https://doi.org/10.1007/978-981-10-7185-0_8.

[3] A. Schütze, T. Baur, M. Leidinger, W. Reimringer, R. Jung, T. Conrad, T. Sauerwald, Highly Sensitive and Selective VOC Sensor Systems Based on Semiconductor Gas Sensors: How to?, Environments. 4 (2017) 20. https://doi.org/10.3390/environments4010020.

[4] E. Hong-Geller, S. Adikari, Volatile Organic Compound and Metabolite Signatures as Pathogen Identifiers and Biomarkers of Infectious Disease, in: Biosensing Technol. Detect. Pathog. - A Prospect. W. Rapid Anal., InTech, 2018. https://doi.org/10.5772/intechopen.72398.

[5] K.M. Tripathi, T. Kim, D. Losic, T.T. Tung, Recent advances in engineered graphene and composites for detection of volatile organic compounds (VOCs) and non-invasive diseases diagnosis, Carbon N. Y. 110 (2016) 97–129. https://doi.org/10.1016/j.carbon.2016.08.040.

[6] K. Wilkins, MICROBIAL VOC (MVOC) IN BUILDINGS , THIER PROPERTIES AND POTENTIAL USE, (2002) 431–436.

[7] Y. Wang, Y. Li, J. Yang, J. Ruan, C. Sun, Microbial volatile organic compounds and their application in microorganism identification in foodstuff, TrAC Trends Anal. Chem. 78 (2016) 1–16. https://doi.org/10.1016/j.trac.2015.08.010.

[8] E. Duffy, A. Morrin, Trends in Analytical Chemistry Endogenous and microbial volatile organic compounds in cutaneous health and disease, Trends Anal. Chem. 111 (2019) 163–172. https://doi.org/10.1016/j.trac.2018.12.012.

[9] C. Pasquarella, O. Pitzurra, A. Savino, The index of microbial air contamination, (2000) 241–256. https://doi.org/10.1053/jhin.2000.0820.

[10] S. Garcia-alcega, Z. Ahmad, R. Ferguson, C. Whitby, A.J. Dumbrell, I. Colbeck, D. Gomes, S. Tyrrel, F. Coulon, Trends in Analytical Chemistry Fingerprinting outdoor air environment using microbial volatile organic compounds (MVOCs)

e A review, Trends Anal. Chem. 86 (2017) 75–83. https://doi.org/10.1016/j.trac.2016.10.010.

[11] A. Wilson, Advances in Electronic-Nose Technologies for the Detection of Volatile Biomarker Metabolites in the Human Breath, Metabolites. 5 (2015) 140–163. https://doi.org/10.3390/metabo5010140.

[12] A.Y. Katukiza, M. Ronteltap, P. Van Der Steen, J.W.A. Foppen, P.N.L. Lens, Quantification of microbial risks to human health caused by waterborne viruses and bacteria in an urban slum, (2014) 447–463. https://doi.org/10.1111/jam.12368.

[13] Z. Zhu, L. Zheng, S. Zheng, J. Chen, X. Xing, D. Feng, D. Yang, Multichannel pathway-enriched mesoporous NiO nanocuboids for the highly sensitive and selective detection of 3-hydroxy-2-butanone biomarkers, J. Mater. Chem. A. 7 (2019) 10456–10463. https://doi.org/10.1039/C9TA01013K.

[14] F. Lough, J.D. Perry, S.P. Stanforth, J.R. Dean, Trends in Analytical Chemistry Detection of exogenous VOCs as a novel in vitro diagnostic technique for the detection of pathogenic bacteria, Trends Anal. Chem. 87 (2017) 71–81. https://doi.org/10.1016/j.trac.2016.12.004.

[15] A. Filipiak W., Sponring A., Filipiak A., Baur, M., Clemens A., Wiesenhofer, H., Margesin, R., Nagis M., Troppmair, J., Interpretation of Breath Analysis Data, 2013.

[16] L.D.J. Bos, P.J. Sterk, M.J. Schultz, Volatile Metabolites of Pathogens : A Systematic Review, 9 (2013) 1–8. https://doi.org/10.1371/journal.ppat.1003311.

[17] A.W. Boots, Identification of microorganisms based on headspace analysis of volatile organic compounds by gas chromatography – mass spectrometry, 027106 (n.d.). https://doi.org/10.1088/1752-7155/8/2/027106.

[18] F. Lough, J.D. Perry, S.P. Stanforth, J.R. Dean, Detection of exogenous VOCs as a novel in vitro diagnostic technique for the detection of pathogenic bacteria, TrAC Trends Anal. Chem. 87 (2017) 71–81. https://doi.org/10.1016/j.trac.2016.12.004.

[19] Z. Zhu, L. Zheng, S. Zheng, J. Chen, X. Xing, D. Feng, D. Yang, Multichannel Pathways-Enriched Mesoporous NiO Nanocuboids for Highly Sensitive and Selective Detection of 3-Hydroxy-2-Butanone Biomarkers, J. Mater. Chem. A. 7 (2019) 10456–10463. https://doi.org/10.1039/C9TA01013K.

[20] N. BARSAN, D. KOZIEJ, U. WEIMAR, Metal oxide-based gas sensor research:

How to?, Sensors Actuators B Chem. 121 (2007) 18–35. https://doi.org/10.1016/j.snb.2006.09.047.

[21] G. Korotcenkov, Metal oxides for solid-state gas sensors: What determines our choice?, Mater. Sci. Eng. B. 139 (2007) 1–23. https://doi.org/10.1016/j.mseb.2007.01.044.

[22] A. Dey, Semiconductor metal oxide gas sensors: A review, Mater. Sci. Eng. B Solid-State Mater. Adv. Technol. 229 (2018) 206–217. https://doi.org/10.1016/j.mseb.2017.12.036.

[23] A.A. Tomchenko, G.P. Harmer, B.T. Marquis, J.W. Allen, Semiconducting metal oxide sensor array for the selective detection of combustion gases, Sensors Actuators, B Chem. 93 (2003) 126–134. https://doi.org/10.1016/S0925-4005(03)00240-5.

[24] S.Y. Jeong, J.S. Kim, J.H. Lee, Rational Design of Semiconductor-Based Chemiresistors and their Libraries for Next-Generation Artificial Olfaction, Adv. Mater. 2002075 (2020) 1–47. https://doi.org/10.1002/adma.202002075.

[25] R.C. Korošec, P. Bukovec, Sol-Gel Prepared NiO Thin Films for, Acta Chim. Slov. 53 (2006) 136–147.

[26] C. Wu, S. Deng, H. Wang, Y. Sun, J. Liu, H. Yan, Preparation of Novel Three-Dimensional NiO/Ultrathin Derived Graphene Hybrid for Supercapacitor Applications, (2014).

[27] A. Kumar Rai, L. Tuan Anh, C.J. Park, J. Kim, Electrochemical study of NiO nanoparticles electrode for application in rechargeable lithium-ion batteries, Ceram. Int. 39 (2013) 6611–6618. https://doi.org/10.1016/j.ceramint.2013.01.097.

[28] C.A. Zito, T.M. Perfecto, C.S. Fonseca, D.P. Volanti, Effective reduced graphene oxide sheets/hierarchical flower-like NiO composites for methanol sensing under high humidity, New J. Chem. 42 (2018) 8638–8645. https://doi.org/10.1039/c8nj01061g.

[29] H. Wang, J. Gao, Z. Li, Y. Ge, K. Kan, K. Shi, One-step synthesis of hierarchical α-Ni(OH)2 flowerlike architectures and their gas sensing properties for NOx at room temperature, CrystEngComm. 14 (2012) 6843–6852. https://doi.org/10.1039/c2ce25553g.

[30] L. Xu, Y.S. Ding, C.H. Chen, L. Zhao, C. Rimkus, R. Joesten, S.L. Suib, 3D flowerlike α-nickel hydroxide with enhanced electrochemical activity synthesized

by microwave-assisted hydrothermal method, Chem. Mater. 20 (2008) 308–316. https://doi.org/10.1021/cm702207w.

[31] J. Zhang, X. Liu, G. Neri, N. Pinna, Nanostructured Materials for Room-Temperature Gas Sensors, Adv. Mater. 28 (2016) 795–831. https://doi.org/10.1002/adma.201503825.

[32] J. Fu, C. Zhao, J. Zhang, Y. Peng, E. Xie, Enhanced gas sensing performance of electrospun Pt-functionalized NiO nanotubes with chemical and electronic sensitization, ACS Appl. Mater. Interfaces. 5 (2013) 7410–7416. https://doi.org/10.1021/am4017347.

[33] M.E. Franke, T.J. Koplin, U. Simon, Metal and metal oxide nanoparticles in chemiresistors: Does the nanoscale matter?, Small. 2 (2006) 36–50. https://doi.org/10.1002/smll.200500261.

2 Effect of Ag on NiO derived from α-nickel hydroxide obtained by the microwave-assisted solvothermal method for the detection of 3-methyl-1-butanol

Abstract

In this chapter, the synthesis of two different materials derived from α-$Ni(OH)_2$ was carried out, NiO and Ag/NiO. Then, characterizations were performed for morphology studies, confirmation of the material obtained and its purity. X-ray diffraction and Fourier-transform infrared spectroscopy indicated the single-phase formation of the material. In addition, the energy dispersive X-ray microanalysis confirms the presence of Ag in the sample. Then, VOC-sensing tests were carried out for the NiO and Ag/NiO 5%. NiO presented an optimum operating temperature at 250 °C and a maximum response of ~2.70 for 100 ppm 3-methyl-1-butanol, compared to the second-best response, ethanol, which showed a response of 1.40 times greater. The Ag/NiO 5% presented a maximum response of ~2.60 for 100 ppm 3-methyl-1-butanol, when compared to the second-best response, ethanol, showed a response of 1.66 times greater. Furthermore, Ag/NiO 5% showed an optimum operating temperature at 200 °C, lower than that of NiO, positively influencing the energy-saving and facilitating possible miniaturization of the system.

Keywords: Microbial volatile organic compounds. α-Nickel hydroxide. Nickel oxide. Silver decorating. Nanocomposite. Gas sensor. 3-Methyl-1-butanol.

2.1 Introduction

Microorganisms are widely studied due to the risks they can cause in human activities[1], as in food spoilage[2] and pathogenicity[3-6] that directly influence in economy and health fields[7]. Some of the contamination routes by microorganisms occur through ingestion due to contaminated potable water, wastewater, soil, and contaminated food sources[8]. Different pathogens produce specific VOC profiles. The analysis of these particular profiles allows VOC's correlation with indications of specific diseases and infections[9].

Among gas sensors, SMOs are the most studied sensor group[10]. SMOs use as reaction mechanisms, oxidation of the studied mVOCs due to oxygen species adsorbed on the material's surface, which causes a hole accumulation layer (for p-type metals)[11]. Among SMOs types, p-type SMOs usually have an inadequate response as a sensor than n-type SMOs, making it difficult to commercialize. So, there is an active research area to increase the performance of these sensors.

NiO is a p-type semiconductor with a bandgap in the range of 3.6–4.0 eV[12], known for its physical stability and excellent electrical properties and the subject of few studies for application in sensors[13,14], which makes it a good alternative for modifications and research as a gas sensor.

α-$Ni(OH)_2$ is a polymorph, hydroxyl-deficient with an interlayer distance of approximately 7 Å, where contains intercalated anions and water molecules, resulting in interlayer chemistry and electrochemical activity. Besides, the α-$Ni(OH)_2$ structure can be easily transformed in NiO, exploring characteristics such as surface area and morphology, directly influencing SMO's performance as a sensor[15,16].

The functionalization of SMO with noble metals (e.g., Ag, Pt) is already confirmed as an effective method to promote surface sensing reactions. The positive effects range from decreasing the optimum working temperature to increasing the selectivity and sensitivity. Silver, decorating the material, contributes to the application of SMO as a sensor through chemical and electrical sensitizing effects[17,18]. Contributions occur by increasing the number of oxygen adsorbed, now on the metal surface or at the metal-SMO interface, catalytic activation by activating oxygen and offering new adsorption sites[18].

In this work, NiO and Ag/NiO 5% derived from α-$Ni(OH)_2$ were successfully prepared. After, different amounts of Ag were deposited on the NiO material. The structures were then chemically and morphologically characterized. Lastly, the VOC-

sensing properties such as selectivity, sensitivity, and NiO and Ag/NiO operating temperature were obtained.

2.2 Experimental section

2.2.1 Preparation of NiO from α-$Ni(OH)_2$

For this synthesis, the microwave-assisted solvothermal method was used. Initially, two solutions were prepared, one of 2 mmol nickel(II) nitrate hexahydrate ($Ni(NO_3)_2.6H_2O$) Sigma-Aldrich, ≥ 98.5%) in 40 mL of methanol and the other 8 mmol 2-methylimidazole (2-MeIM Sigma-Aldrich, ≥ 99%) in 40 mL of methanol, both under continuous stirring. Then, the solutions were mixed and kept under stirring for five minutes. The mixture was transferred to a sealed polytetrafluoroethylene (Teflon) reactor with a capacity of 100 mL. The reactor was heated to 140 °C for 1 hour by microwave (2.45 GHz / 800W). After naturally cooling, the reactor was opened at 50 °C. The product was centrifuged (7500 RPM), washed three times with methanol, and dried at 60 °C overnight. Finally, the product (α-$Ni(OH)_2$) was calcined at 350 ° C for 3 hours with a heating rate of 5 ° C min^{-1}.

2.2.2 Ag/NiO preparation

A 2 mg mL^{-1} aqueous dispersion of NiO was prepared using an ultrasonic bath for 30 min. Different quantities of $AgNO_3$ (10 mg mL^{-1}) were added to de dispersion, under stirring, to obtain the final Ag amount of 0.5, 1, 2, and 5 wt% in the Ag/NiO structures. The dispersion was stirred for 10 min. The calculated amount of sodium borohydride ($NaBH_4$ Sigma-Aldrich, ≥ 98%) was added, and the dispersion was stirred for 5 min. Double the number of mols of $AgNO_3$ was used to calculate the mass of $NaBH_4$. The number of moles of $AgNO_3$ was obtained using the necessary mass of Ag for the calculations. The final product was centrifuged and washed several times with water and ethanol. Finally, the material was dried at 60 °C overnight.

2.2.3 Characterization

The sample was characterized by X-ray powder diffraction (XRD, Rigaku MiniFlex 300), using Cu Kα radiation (λ = 1.5418 Å) operated at 30 kV and 10 mA. The samples were analyzed in the 2θ range of 10-90° at a scanning rate of 2°min^{-1} with a step size of 0.1°. Field-emission scanning electron microscopy (FESEM, JEOL JSM-7500F) were operated at 2kV to obtain images and at 10kV for X-ray dispersive energy

spectroscopy (EDX). For Fourier transformed infrared (FTIR) spectra, the sample was analyzed as powder by a Perkin Elmer spectrophotometer Spectrum Two. The X-ray photoelectron spectroscopy (XPS) spectra were recorded on a Thermo Scientific K-alpha X-ray photoelectron spectrometer using Al Kα radiation (1486.6 keV). The binding energies were calibrated with reference to the C 1s peak (284.8 eV). The Scherrer equation ($Dp = (0.94 \times \lambda) / (\beta \times \cos\theta)$) estimated the crystallite sizes of the samples to the full width at half-maximum (fwhm) of the (111), (200), and (220) peaks. Crystallinity was obtained using the Origin software, using only the NiO peaks for its calculation as the ratio of (peaks area/total area) x 100%, except α-$Ni(OH)_2$, where all the peaks present in the XRD were used.

2.2.4 VOCs-sensing measurements

A dispersion of the material was prepared in isopropanol and deposited in an alumina substrate with interdigitated gold arrays (200 µm Au fingers spaced 200 µm apart). The electrode was heated at 400 °C for 1 h. Afterward, the sensor was placed inside the test chamber and heated at the desired operating temperature. The electrical resistance variations were measured after VOC exposure using a high-voltage source-measure unit (Keithley SourceMeter 2400), applying a voltage of 5 V. The VOCs were injected into the test chamber using a syringe. Then the chamber was cleaned using an airflow of 250 mL min^{-1}. The sensor response was defined as the ratio R_g/R_a, where R_g and R_a show resistance after VOC exposure and in the air, respectively. In addition, the VOCs sensing studies were also conducted at a relative humidity (RH) of 56%, measured by a thermohygrometer (HANNA, HI9564 model). To control de RH, the airflow pass through a closed vessel containing a saturated solution of NaBr before entering the test chamber, so controlling the RH of the system.

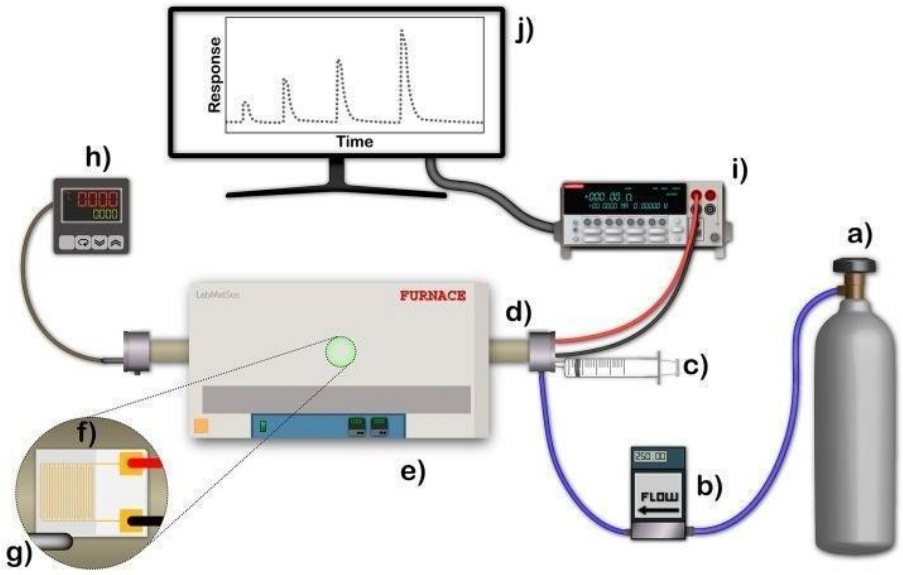

Figure 3. Schematic illustration of the VOC-sensing measurement setup. a) air cylinder; b) flow meter; c) VOC injection syringe; d) septum to insert the VOC; e) tubular oven; f) interdigital alumina electrode containing deposited sample; g) thermocouple; h) PID temperature controller; i) Keithley Source Measure Unit, and j) visualization of the resistance variation with time. **Reference:** OLIVEIRA, T.N.T. et al, 2020[17].

2.3 Results and discussion

The XRD pattern characteristic for α-$Ni(OH)_2$ is shown in Figure 4. The peaks shown to overlap with those present in JCPDS 38-715, referring to a R (0) rhombohedral crystallographic structure, the peaks at 2θ are in 11.3 °; 22.59 °; 34.12 °; 38.25 ° and 59.5° which were indexed to the following crystalline planes (003), (006), (012), (015) and (110).

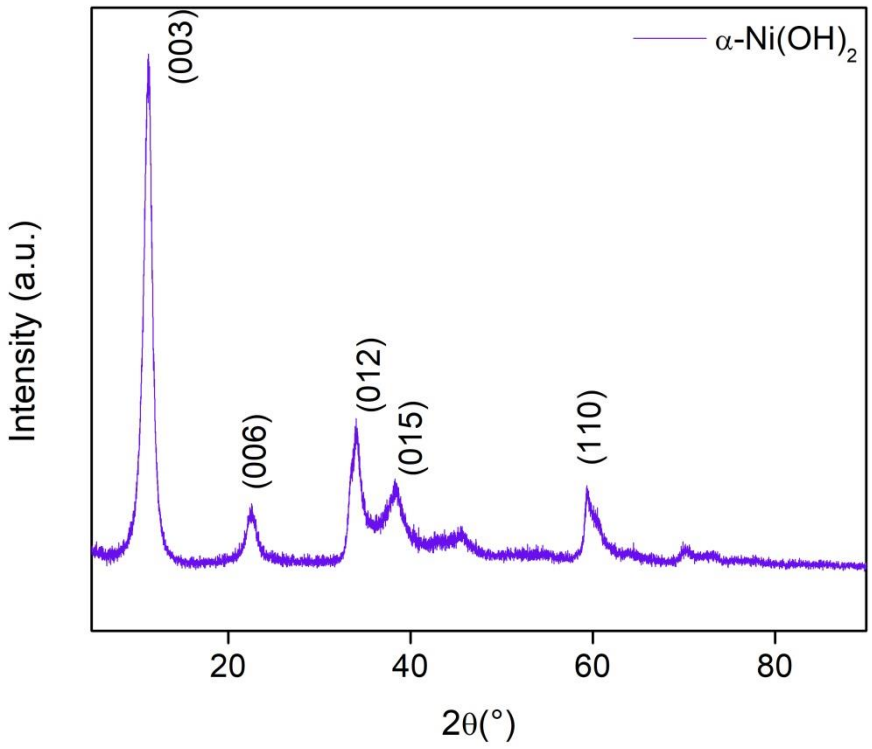

Figure 4. XRD patterns of α-$Ni(OH)_2$. **Reference:** Elaborated by the author.

The XRD pattern obtained for the NiO sample is shown in Figure 5. The sample presented an Fm-3m (225) cubic crystallographic structure for NiO (JCPDS 78-643), as the positions can see it of the peaks at 2θ, 37.3 °; 43.3 °; 62.8 °; 75.4 ° and 79.4 ° which were indexed to the following crystalline planes (111), (200), (220), (311) and (222).

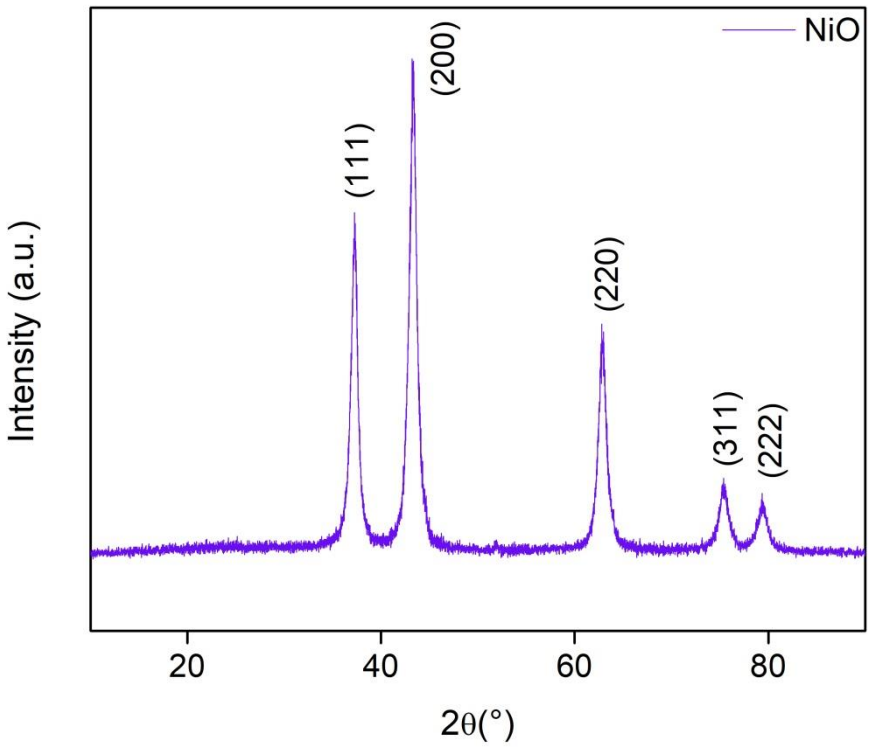

Figure 5. XRD patterns of NiO. **Reference:** Elaborated by the author.

Figure 6, presents the obtained XRD pattern of the Ag/NiO samples. The NiO peaks of each sample presented at 2θ, 37.3 °; 43.3 °; 62.8 °; 75.4 ° and 79.4 ° agreed with the shown in Figure 5, according to the cubic crystallographic structure (JCPDS 78-643). Due to the small amount of Ag in the samples, NiO masks the silver peaks. However, in the sample with 5wt% Ag, following the JCPDS 87-720 pattern, its already possible to visualize and identify the peaks present at 2θ, 38.10°; 64.47° and 77.48°, which refers to metallic silver with an Fm-3m (225) cubic crystallographic structure.

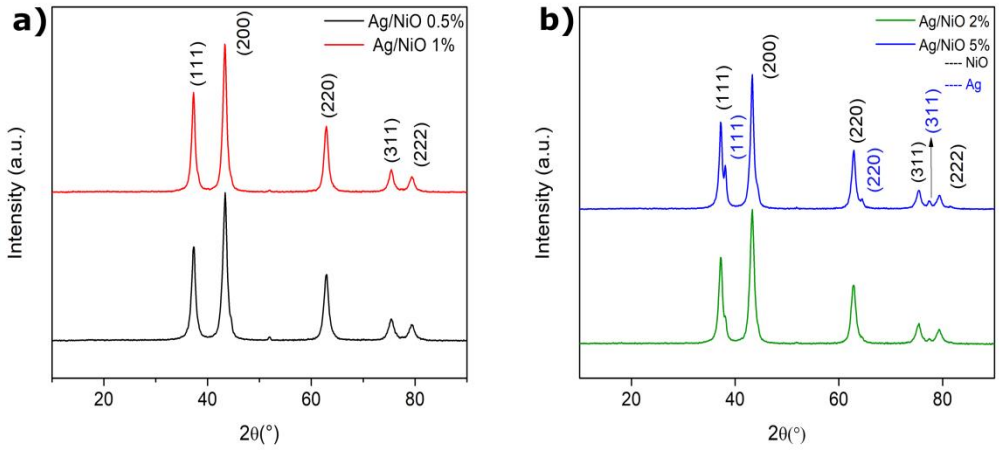

Figure 6. a) XRD patterns of 0.5% Ag/NiO and 1% Ag/NiO. b) XRD patterns of 2% Ag/NiO and 5% Ag/NiO. **Reference:** Elaborated by the author.

Table 1 shows the data for crystallite size and crystallinity of the samples. Initially, for the degree of crystallinity, the addition of Ag in small amounts does not interfere with crystallinity; however, when a more considerable amount of Ag was inserted, a significant decrease in crystallinity was observed, as presented by the 5% Ag/NiO sample. Similarly, comparing the averages of the crystallite size, it is possible to keep that the result does not follow a pattern as the Ag is added to the sample. However, when the calculation is made for a sample with a higher percentage of silver, the average crystallite size increases, obtaining a value of 13.60 nm.

Table 1. Crystallite size and crystallinity of the samples.

Sample	Average crystallite size	Crystallinity
α-$Ni(OH)_2$	6.29 nm	36.9%
NiO	10.19 nm	86.8%
0.5% Ag/NiO	9.85 nm	85.7%
1% Ag/NiO	11.11 nm	86%
2% Ag/NiO	10.01 nm	83.2%
5% Ag/NiO	13.60 nm	76.4%

Reference: Elaborated by the author.

The FESEM images of *α-Ni(OH)₂*, Figure 7a,b,c, revealed a cluster of particles composed of a two-dimensional (2D) petal-like morphology. When comparing with the FESEM images of NiO, Figure 7d,e,f, of greater magnification, Figure 7f, it is possible to observe the presence of pores in the material that were not seen before, Figure 7d. The pores come from the precursor structure after calcination and may thus provide a higher surface area to the material. Obtaining the desired morphology is an essential step in developing the sensor material due to the importance that a large surface area has, causing more significant contact between the material and VOCs.

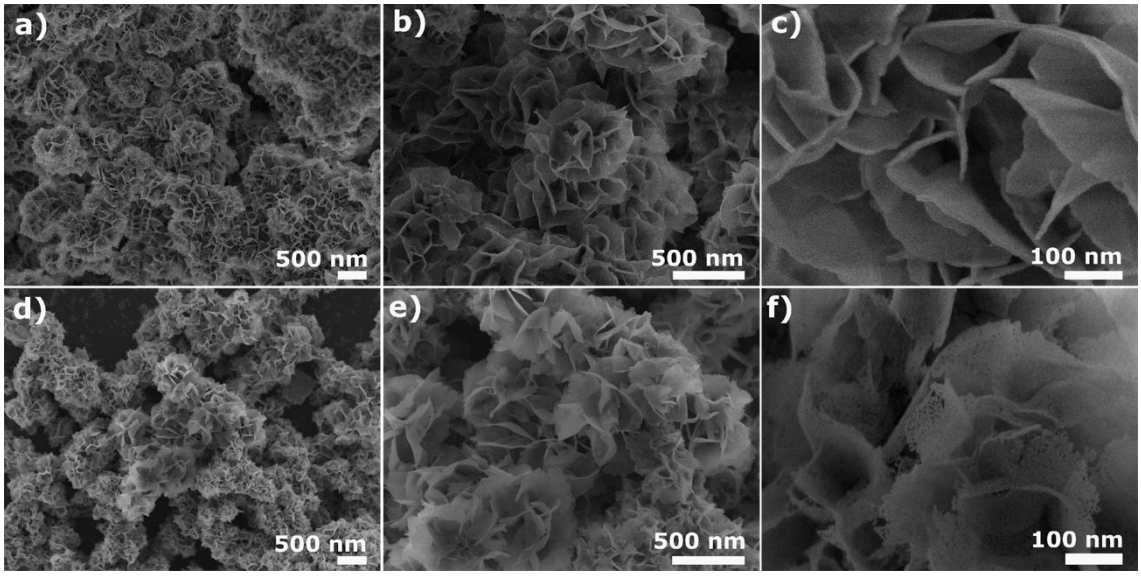

Figure 7. FESEM images (a,b,c) *α-Ni(OH)₂* and (d,e,f) NiO with different magnifications. **Reference:** Elaborated by the author.

As shown in Figure 8, there were no significant changes in the samples' morphology with Ag. The images obtained also showed the petal-like morphology with pores in its structure. FESEM does not allow the visualization of Ag in the material. In this way, for a chemical characterization, EDX analysis was performed.

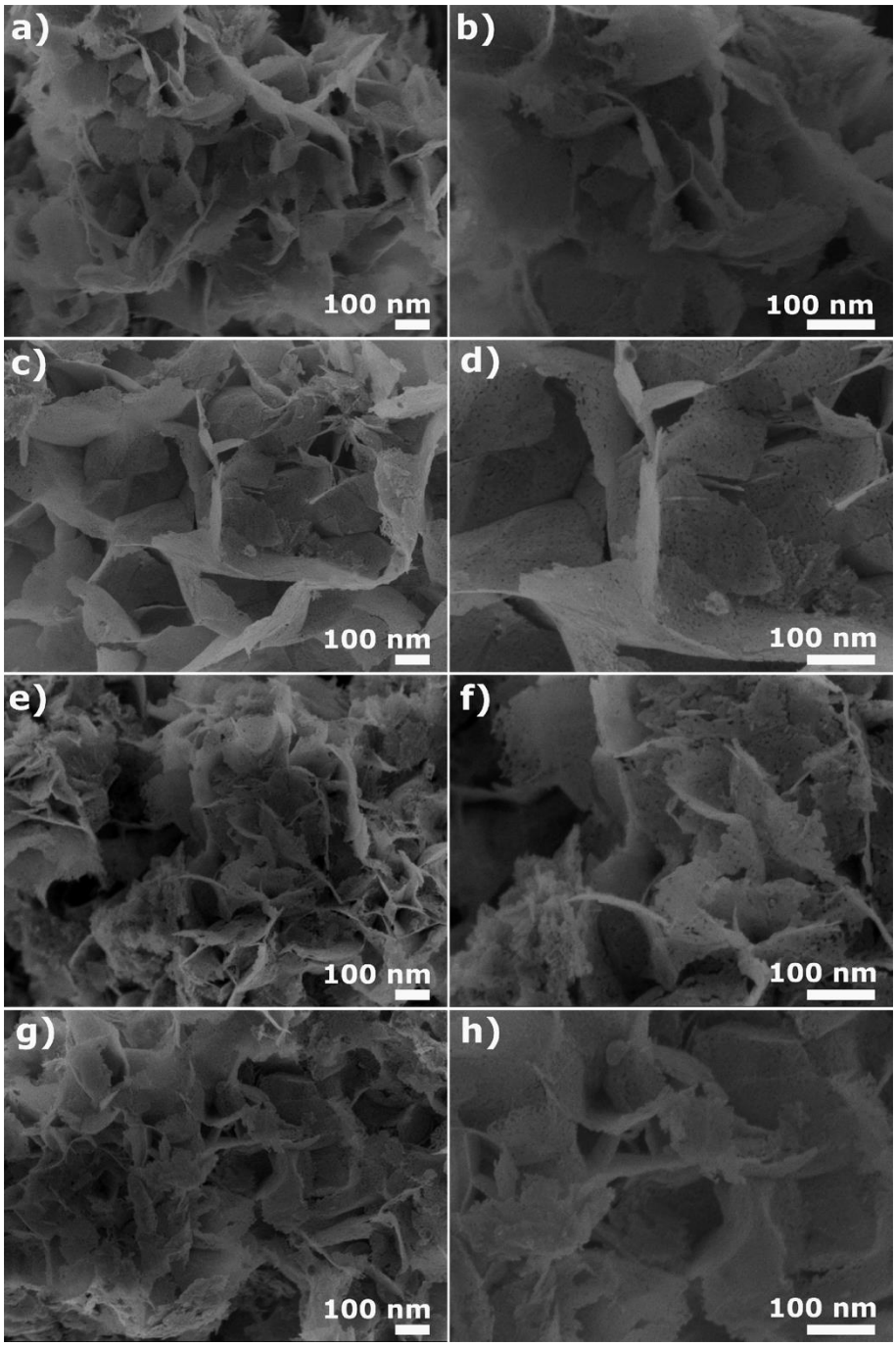

Figure 8. FESEM images a,b) 0.5% Ag/NiO; c,d) 1% Ag/NiO; e,f) 2% Ag/NiO; 5% Ag/NiO, with different magnifications. **Reference:** Elaborated by the author.

EDX analysis was carried out in NiO and 5% Ag/NiO due to the original material and the modification with a more significant amount of Ag, which may facilitate the visualization of its respective peak. In the EDX spectrum, Figure 9, it is possible to observe a maximum of five different peaks, namely, oxygen (O), nickel (Ni) and silicon (Si), and silver (Ag). Four of them are present in both spectra. The Ni and O peaks come from NiO, while the Si peak comes from the substrate used for analysis.

The peak of Ag, Figure 9b, comes from the modification previously made in the material to obtain Ag/NiO. The significant difference in intensity between the Ni and Ag peaks is due to the small amounts of Ag (5%) in the samples. No peak of contamination is observed, ensuring the purity of the materials.

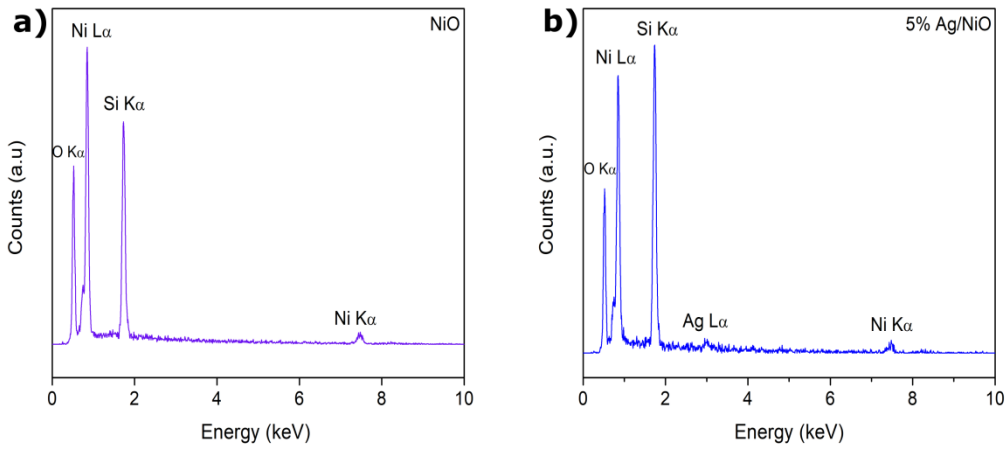

Figure 9. a) EDX spectrum of NiO and b) 5% Ag/NiO. **Reference:** Elaborated by the author.

The FTIR spectra of NiO and the different Ag/NiO samples are shown in Figure 10. The spectra obtained for the Ag/NiO samples were similar to those presented by the NiO. The peak at 533 was assigned to the stretching vibration mode of Ni–O[19]. The broadband present in 3450 cm^{-1} and 1637cm^{-1} can be given to the vibrations' stretching and bending of water molecules physically adsorbed on NiO[19,20]. The additional low intense peak at 2980 cm^{-1} can be attributed to C-H bending vibrations, in addition to weak bands at 1390-800 cm^{-1} range that can be ascribed to the vibration of the absorbed CO_2 molecules and small residues of the reagents used to synthesize α-$Ni(OH)_2$[21].

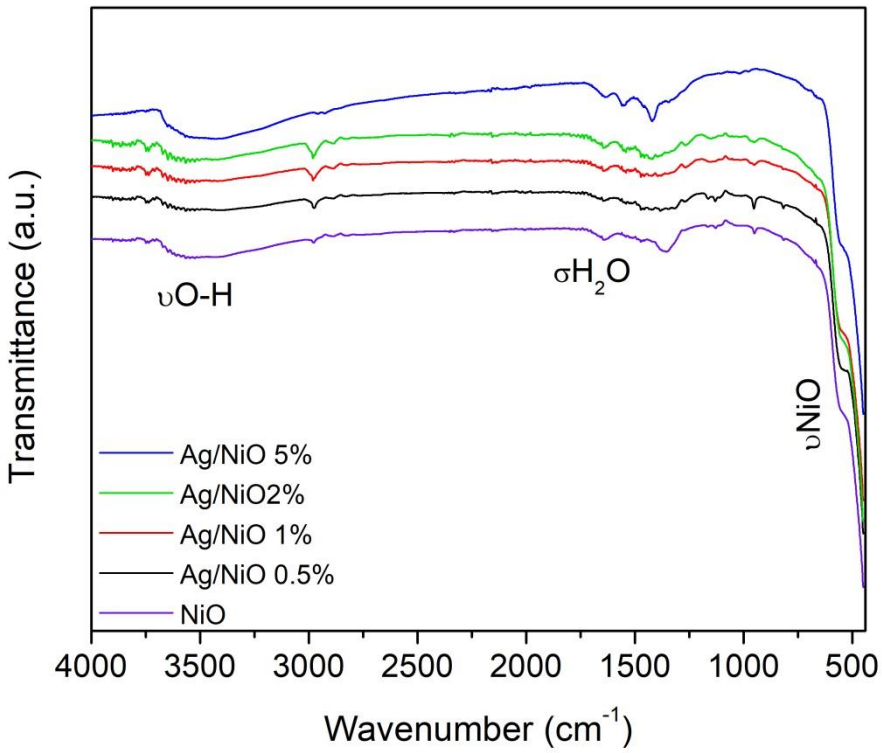

Figure 10. FTIR spectra of NiO; 0.5% Ag/NiO ; 1% Ag/NiO; 2% Ag/NiO and 5% Ag/NiO. **Reference:** Elaborated by the author.

XPS technique was performed to obtain Ag/NiO 5% surface chemical composition and electronic structure. Figure 11a, presents the survey XPS spectra of the material, only peaks related to O, Ni, Ag, and C were detected, the latter being due to the contact of the sample with atmospheric air. Figure 11b, shows the high-resolution spectra of O 1s, composed of four different components at 529.2 (O_1) eV, 530.6 (O_2) eV, 532.1 (O_3) eV, and 533.3 (O_4) eV. The binding energy presents in (O_1) can be assigned to a typical metal-oxygen bond in NiO (O_1)[19,22,23], oxygen-deficient regions (O_2)[22,23], oxygen from residual organic matter present in the sample (O_3)[24] and physical and chemosorbed molecular water (O_4)[25-27]. The high-resolution spectra of Ni 2p, presented in Figure 11c, suggested four easily discernible features, two major peaks can be observed at ~853.8 eV and 872.4 eV, corresponding to Ni $2p_{3/2}$ and Ni $2p_{1/2}$, respectively. In addition, two satellite peaks were also observed in the spectra at ~861 eV and ~879 eV, corresponding to Ni $2p_{3/2}$ and Ni $2p_{1/2}$. These significant and satellite peaks are typical of NiO[15]. Figure 11d, shows the high-resolution spectra of

Ag, which presents two peaks at 368.2 and 374.1 eV, referring to Ag $3d_{5/2}$ and Ag $3d_{3/2}$, respectively, indicating the presence of metallic silver in the material [28].

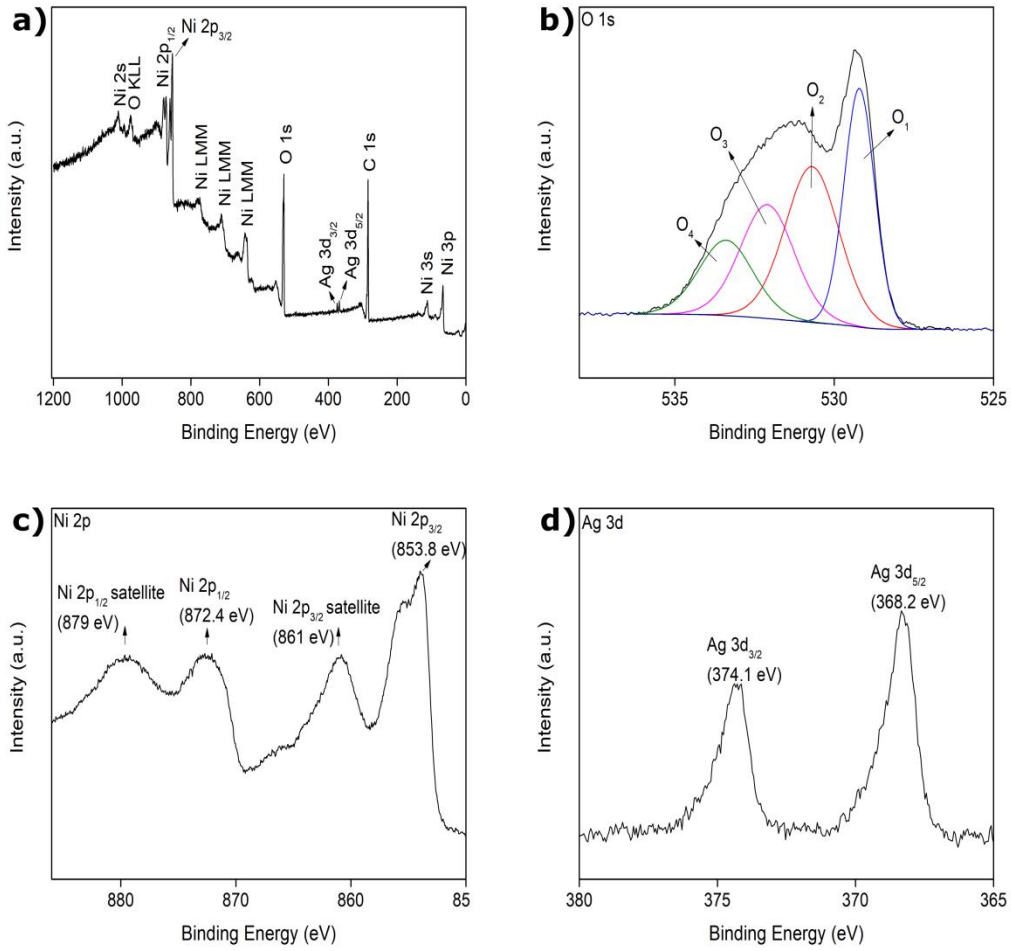

Figure 11. (a) Survey XPS spectra of the sample. High-resolution XPS spectra of (b) O 1s, (c) Ni 2p, and (d) Ag 3d. **Reference:** Elaborated by the author.

To characterize NiO VOC-sensing properties, the response to 100 ppm 3-methyl-1-butanol, a type of mVOC, was measured at different temperatures, Figure 12a. The maximum signal can be observed at 250 °C. As expected for the semiconductors, the material's resistance decreased as the temperature increased. For selectivity test, six different VOCs were added separately into the chamber at a concentration of 100 ppm, Figure 12b. The NiO sample showed best response for 3-methyl-1-butanol, which is 1.40 times higher than that to ethanol, the second best response of the material.

The sensitivity test was performed by increasing the 3-methyl-1-butanol concentration range from 5 to 200 ppm at the optimum operating temperature. The increase in the concentration of 3-methyl-1-butanol provides an increase in the material's resistance after contact with the volatile, Figure 12c. Thus, providing a more significant response, according to the rise in the concentration of 3-methyl-1-butanol. The NiO showed a response changing from 1.52 to 2.78 for the concentration range 5-200 ppm of 3-methyl-1-butanol, as can be observed in Figure 12d. At 5 ppm the material showed a response of 1.52, being equivalent to 54% of the response presented for the highest concentration, 200 ppm. The material shows a high sensitivity at low concentrations.

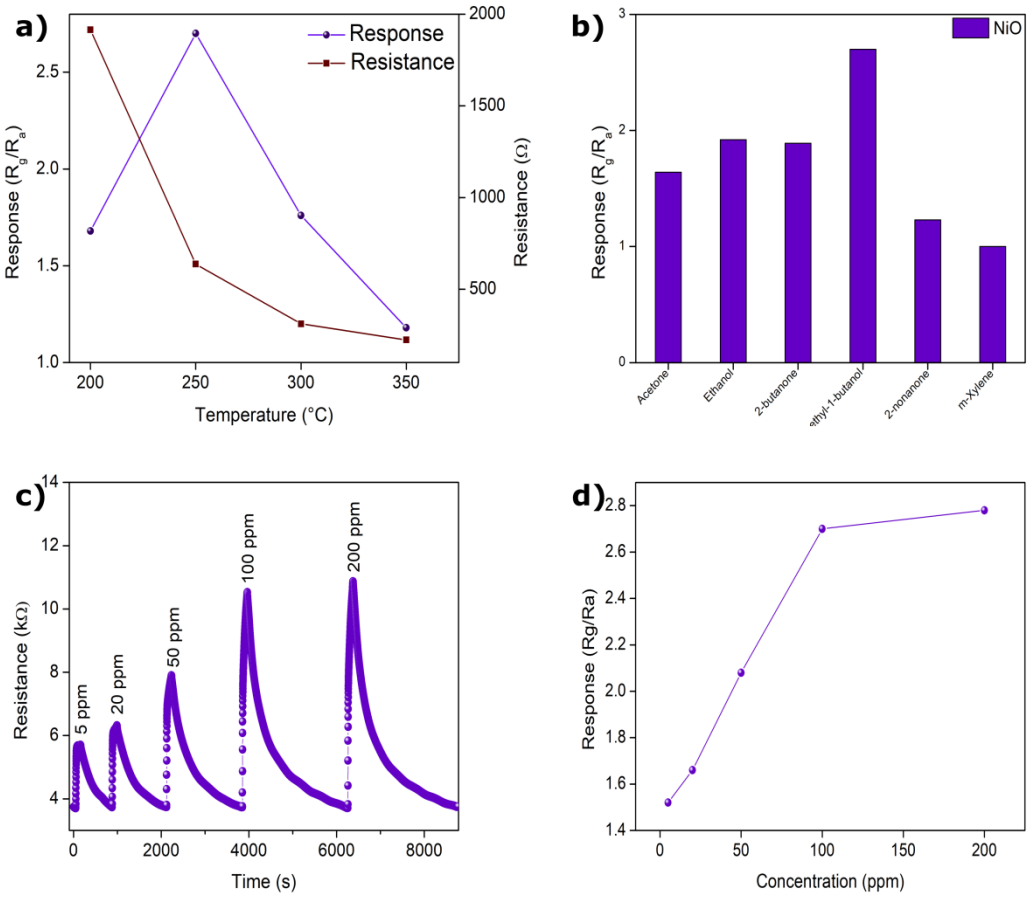

Figure 12. a) Response to 100 ppm 3-methyl-1-butanol of NiO at different operating temperatures (200-350°C), b) response to 100 ppm of different VOCs and mVOCs at the optimum operating temperatures (250 °C), c) resistance changes of NiO upon exposure to 3-methyl-1-butanol in the concentration range of 5-200 ppm, d) response of NiO to 3-methyl-1-butanol in a concentration range of 5-200 ppm. **Reference:** Elaborated by the author.

The same selectivity test was performed for the Ag/NiO samples, where six different VOCs were added separately in the system at a concentration of 100 ppm. The results are presented in tables S1-S4, referring to Ag/NiO 0.5%, Ag/NiO 1%, Ag/NiO 2% and Ag/NiO 5%, respectively. It was possible to observe that Ag/NiO 5% was the material that presented the best response among the different samples, Figure 13.

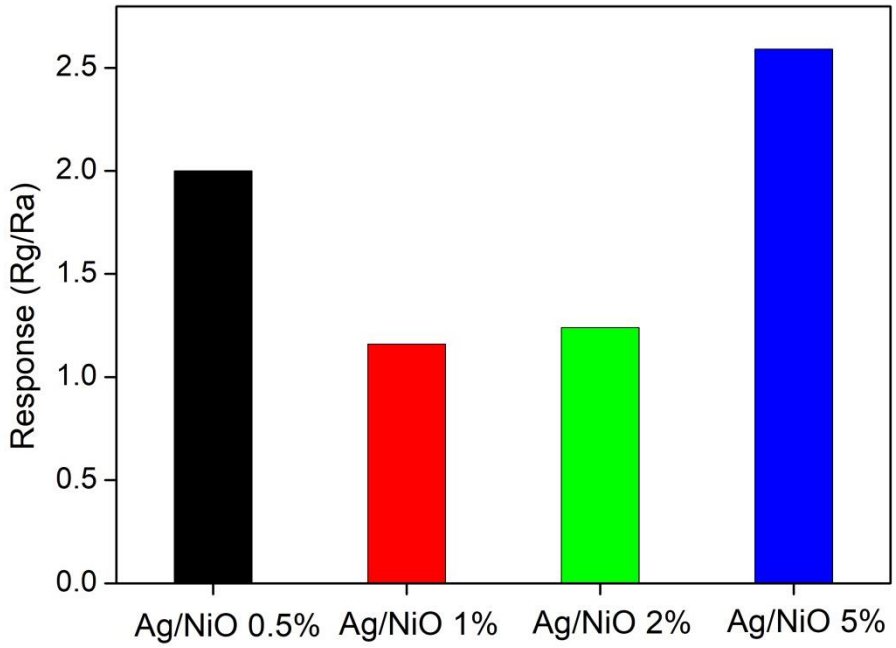

Figure 13. Response to 100 ppm 3-methyl-1-butanol of NiO with different percentages of silver.
Reference: Elaborated by the author.

In general, the Ag/NiO 5% sample has a response similar to NiO; the main change is observed in the decrease of the optimum operating temperature, Figure 14a, which is now 200 °C. The 5% Ag/NiO showed the best response for 3-methyl-1-btutanol, Figure 14b, which is 1.66 times higher than that to ethanol, the second best response of the sample. It is important to note that the Ag in the material presented some characteristics such as a decrease in the optimum operating temperature and an increase in selectivity since the detection response to 3-methyl-1-butanol is now 40% higher than for ethanol.

The sensitivity test for Ag/NiO 5%, Figure 14c, was also performed by increasing the 3-methyl-1-butanol concentration range from 5 to 200 ppm at the optimum operating temperature. As expected, the material's response increases as the

concentration of the volatile increases. The response obtained to Ag/NiO 5%, Figure 14d, changes from 1.81 to 2.62 for the concentration range of 5-200 ppm of 3-methyl-1-butanol. At 5 ppm, the material showed a response of 1.81, being equivalent to 69% of the response presented for the highest concentration, 200 ppm. It also showed a high sensitivity at low concentrations, even better than that presented for NiO.

The maximum response values obtained for NiO and Ag/NiO 5% with 100 ppm of 3-methyl-1-butanol are similar, which are 2.70 and 2.60, respectively. The best response was received at two different temperatures, 250 and 200 °C, for NiO and Ag/NiO 5%, respectively. The Ag/NiO 5% maximum response obtained for 3-methyl-1-butanol at 200 °C is attractive due to better selectivity and the lower temperature required for the high signal, influencing the energy-saving and facilitating possible miniaturization of the system.

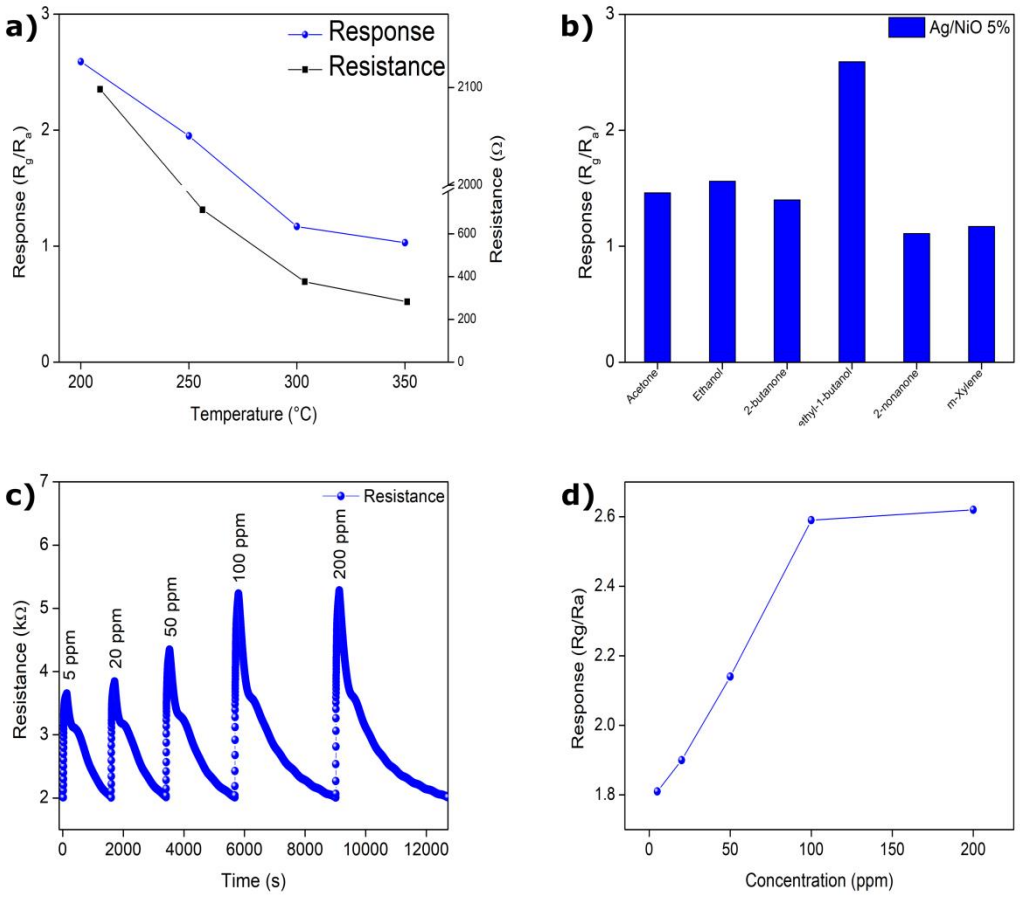

Figure 14. a) Response to 100 ppm 3-methyl-1-butanol of Ag/NiO 5% at different operating temperatures (200-350°C), b) response to 100 ppm of different VOCs and mVOCs at the optimum operating temperatures (200 °C), c) resistance changes of Ag/NiO 5% upon exposure to 3-methyl-1-butanol in a concentration range of 5-200 ppm, d) response of Ag/NiO 5% to 3-methyl-1-butanol in a concentration range of 5-200 ppm. **Reference:** Elaborated by the author.

Both NiO and Ag/NiO, 5% materials, were also subjected to sensing tests to detect 3-methyl-1-butanol in humidity atmosphere at different concentrations, 5 to 200 ppm, with an RH of 56%. NiO and Ag/NiO 5% showed responses similar to those previously presented in low concentrations, with responses of ~1.50 and ~1.87, respectively, at 5 ppm. At 200 ppm, the responses were ~2.29 and ~2.48 for NiO and Ag/NiO 5%, respectively. According to Figure 15, the Ag/NiO 5% maintained high sensitivity for low concentrations, such as 5 ppm, even under humid conditions (56%).

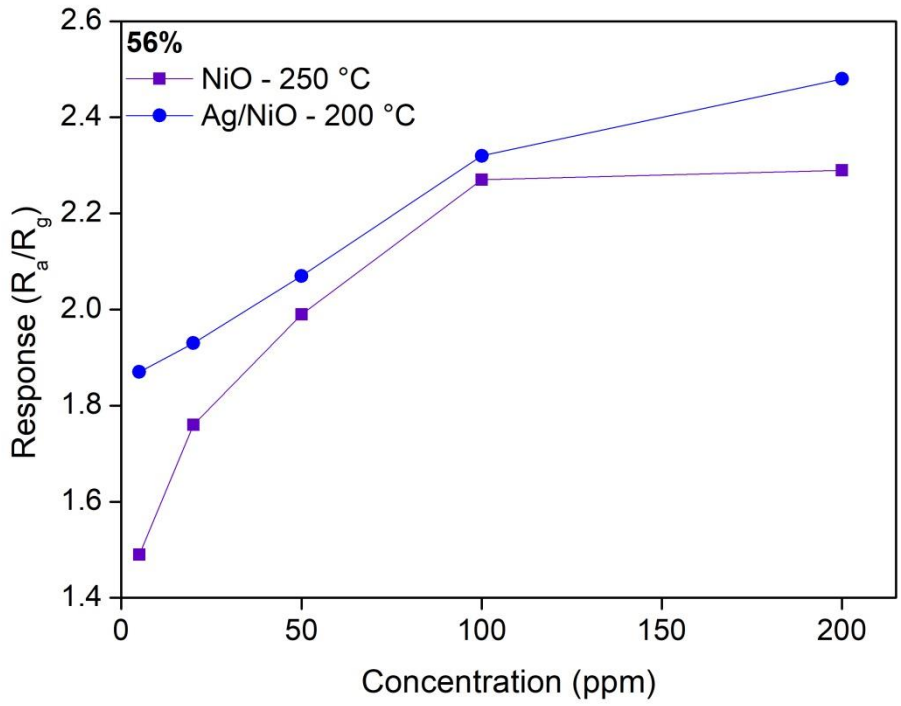

Figure 15. Responses of NiO and Ag/NiO 5% as a function of 3-methyl-1-butanol concentration at a related optimum operating temperature under a wet atmosphere of 56%. **Reference:** Elaborated by the author.

2.4 Conclusion

In this work, two syntheses were presented, the first to obtain NiO and the second to get Ag/NiO in different percentages of Ag. Both were successful, which can be observed in the characterizations of XRD and FTIR, guaranteeing the purity and obtaining of the desired materials. In addition to the confirmation of the presence of Ag through the EDX spectra. It is also possible to observe through the FESEM images obtaining petal-like morphology (2D) for NiO and for Ag/NiO the presence of pores in

addition to the petal-like morphology. mVOC-sensing performance for NiO showed the best response for 3-methyl-1-butanol, a response of ~2.70 at 250 °C, 1.40 times higher than for ethanol, the second-best answer. Ag/NiO showed the best response of ~2.60 at 200 °C, ~1.66 times higher than ethanol. In addition, both materials do not lose their sensitivity in a 56% humid atmosphere. The deposition of silver positively influenced the decrease in the optimum working temperature. It increased the sensitivity of the material to lower concentrations (5 ppm), which facilitates and makes the possible miniaturization of the system more accessible and attractive.

Acknowledgments

The authors thank São Paulo Research Foundation – FAPESP, National Council for Scientific and Technological Development – CNPq, and National Council for the Improvement of Higher Education – CAPES (88882.434462/2019-01). LMA/IQ/Unesp provided FESEM facility.

References

[1] C. Pasquarella, O. Pitzurra, A. Savino, The index of microbial air contamination, (2000) 241–256. https://doi.org/10.1053/jhin.2000.0820.

[2] Y. Wang, Y. Li, J. Yang, J. Ruan, C. Sun, Microbial volatile organic compounds and their application in microorganism identification in foodstuff, TrAC Trends Anal. Chem. 78 (2016) 1–16. https://doi.org/10.1016/j.trac.2015.08.010.

[3] K.M. Tripathi, T. Kim, D. Losic, T.T. Tung, Recent advances in engineered graphene and composites for detection of volatile organic compounds (VOCs) and non-invasive diseases diagnosis, Carbon N. Y. 110 (2016) 97–129. https://doi.org/10.1016/j.carbon.2016.08.040.

[4] E. Duffy, A. Morrin, Trends in Analytical Chemistry Endogenous and microbial volatile organic compounds in cutaneous health and disease, Trends Anal. Chem. 111 (2019) 163–172. https://doi.org/10.1016/j.trac.2018.12.012.

[5] S. Garcia-alcega, Z. Ahmad, R. Ferguson, C. Whitby, A.J. Dumbrell, I. Colbeck, D. Gomes, S. Tyrrel, F. Coulon, Trends in Analytical Chemistry Fingerprinting outdoor air environment using microbial volatile organic compounds (MVOCs) e A review, Trends Anal. Chem. 86 (2017) 75–83. https://doi.org/10.1016/j.trac.2016.10.010.

[6] A. Wilson, Advances in Electronic-Nose Technologies for the Detection of

Volatile Biomarker Metabolites in the Human Breath, Metabolites. 5 (2015) 140–163. https://doi.org/10.3390/metabo5010140.

[7] K. Wilkins, MICROBIAL VOC (MVOC) IN BUILDINGS , THIER PROPERTIES AND POTENTIAL USE, (2002) 431–436

[8] A.Y. Katukiza, M. Ronteltap, P. Van Der Steen, J.W.A. Foppen, P.N.L. Lens, Quantification of microbial risks to human health caused by waterborne viruses and bacteria in an urban slum, (2014) 447–463. https://doi.org/10.1111/jam.12368.

[9] X. Sun, K. Shao, T. Wang, Detection of volatile organic compounds (VOCs) from exhaled breath as noninvasive methods for cancer diagnosis, Anal. Bioanal. Chem. 408 (2016) 2759–2780. https://doi.org/10.1007/s00216-015-9200-6.

[10] A. Dey, Semiconductor metal oxide gas sensors: A review, Mater. Sci. Eng. B Solid-State Mater. Adv. Technol. 229 (2018) 206–217. https://doi.org/10.1016/j.mseb.2017.12.036.

[11] H. Kim, J. Lee, Highly sensitive and selective gas sensors using p-type oxide semiconductors: Overview, Sensors Actuators B Chem. 192 (2014) 607–627. https://doi.org/10.1016/j.snb.2013.11.005.

[12] R.K.Ã. Gupta, K. Ghosh, P.K. Kahol, Fabrication and characterization of NiO / ZnO p – n junctions by pulsed laser deposition, 41 (2009) 617–620. https://doi.org/10.1016/j.physe.2008.10.013.

[13] I. Hotovy, V. Rehacek, P. Siciliano, S. Capone, L. Spiess, Sensing characteristics of NiO thin films as NO 2 gas sensor, 418 (2002) 9–15.

[14] X. Li, X. Zhang, Z. Li, Y. Qian, Synthesis and characteristics of NiO nanoparticles by thermal decomposition of nickel dimethylglyoximate rods, 137 (2006) 581–584. https://doi.org/10.1016/j.ssc.2006.01.031.

[15] H. Wang, J. Gao, Z. Li, Y. Ge, K. Kan, K. Shi, One-step synthesis of hierarchical α-Ni(OH)2 flowerlike architectures and their gas sensing properties for NOx at room temperature, CrystEngComm. 14 (2012) 6843–6852. https://doi.org/10.1039/c2ce25553g.

[16] L. Xu, Y.S. Ding, C.H. Chen, L. Zhao, C. Rimkus, R. Joesten, S.L. Suib, 3D flowerlike α-nickel hydroxide with enhanced electrochemical activity synthesized by microwave-assisted hydrothermal method, Chem. Mater. 20 (2008) 308–316. https://doi.org/10.1021/cm702207w.

[17] T.N.T. Oliveira, C.A. Zito, T.M. Perfecto, G.M. Azevedo, D.P. Volanti, ZnO

twin-rods decorated with Pt nanoparticles for butanone detection, New J. Chem. 44 (2020) 15574–15583. https://doi.org/10.1039/d0nj03206a.

[18] D. Degler, U. Weimar, N. Barsan, Current Understanding of the Fundamental Mechanisms of Doped and Loaded Semiconducting Metal-Oxide-Based Gas Sensing Materials, ACS Sensors. 4 (2019) 2228–2249.

[19] C.A. Zito, T.M. Perfecto, C.S. Fonseca, D.P. Volanti, Effective reduced graphene oxide sheets/hierarchical flower-like NiO composites for methanol sensing under high humidity, New J. Chem. 42 (2018) 8638–8645. https://doi.org/10.1039/c8nj01061g.

[20] M.A.S.P.C. Muthamizhchelvan, Synthesis and characterization of NiO nanoparticles by sol – gel method, (2012) 728–732. https://doi.org/10.1007/s10854-011-0479-6.

[21] J. Li, F. Luo, Q. Zhao, Z. Li, H. Yuan, D. Xiao, Coprecipitation fabrication and electrochemical performances of coral-like mesoporous NiO nanobars, J. Mater. Chem. A. 2 (2014) 4690–4697. https://doi.org/10.1039/c3ta14694d.

[22] E.L. Ratcliff, J. Meyer, K.X. Steirer, A. Garcia, J.J. Berry, D.S. Ginley, D.C. Olson, A. Kahn, N.R. Armstrong, Evidence for near-Surface NiOOH Species in Solution-Processed NiO, Chem. Mater. 23 (2011) 4988–5000. http://pubs.acs.org/doi/abs/10.1021/cm202296p.

[23] C. Wang, X. Cui, J. Liu, X. Zhou, X. Cheng, P. Sun, X. Hu, X. Li, J. Zheng, G. Lu, Design of Superior Ethanol Gas Sensor Based on Al-Doped NiO Nanorod-Flowers, ACS Sensors. 1 (2016) 131–136. https://doi.org/10.1021/acssensors.5b00123.

[24] A.N. Mansour, Characterization of α-Ni(OH)2 by XPS, Surf. Sci. Spectra. 3 (1994) 279–286. https://doi.org/10.1116/1.1247757.

[25] H. Jiang, Y. Guo, T. Wang, P.L. Zhu, S. Yu, Y. Yu, X.Z. Fu, R. Sun, C.P. Wong, Electrochemical fabrication of Ni(OH)2/Ni 3D porous composite films as integrated capacitive electrodes, RSC Adv. 5 (2015) 12931–12936. https://doi.org/10.1039/c4ra15092a.

[26] M.A. Peck, M.A. Langell, Comparison of nanoscaled and bulk NiO structural and environmental characteristics by XRD, XAFS, and XPS, Chem. Mater. 24 (2012) 4483–4490. https://doi.org/10.1021/cm300739y.

[27] Y. Tong, H. Mao, P. Chen, Q. Sun, F. Yan, F. Xi, Confinement of fluorine anions in nickel-based catalysts for greatly enhancing oxygen evolution activity, Chem.

Commun. 56 (2020) 4196–4199. https://doi.org/10.1039/d0cc01215g.

[28] T. Scientific, XPS Reference, (n.d.). https://xpssimplified.com/periodictable.php (accessed September 9, 2019).

3 General conclusions

The main concepts (e.g., VOC and mVOCs) and principles for understanding the work, the importance, and the need to develop alternatives for detecting these compounds were presented in the first chapter. The reason SMOs are an excellent alternative as a group for detecting mVOCs. Other essential points were also addressed, such as the need and importance of techniques for obtaining materials with a high specific morphology, a characteristic explored by the use of α-$Ni(OH)_2$ as a precursor, which may directly influence the performance of the SMO as a mVOC sensor. Besides the use of Ag for decorating NiO and obtaining possible sensitization reactions which may positively impact the selectivity, sensitivity, and even the material's optimum operating temperature.

In the second chapter, the syntheses for obtaining the materials were presented, in addition to characterizations such as XRD, XPS, FTIR, and FESEM, ensuring the obtaining, purity, and morphology of the desired materials. VOC-sensing tests were also carried out for NiO and Ag/NiO 5%, presenting an optimal working temperature of 250 and 200 °C, respectively. In addition, selectivity of ~2.70 and ~2.60 for 100 ppm of 3-methyl-1-butanol. This response is 1.40 and 1.66 times higher than the compound with the second-best response, ethanol. It was also confirmed that the materials could detect low concentrations and perform their function in humid environments, as shown in the sensitivity graphs.

APÊNDICE A – Response of Ag/NiO samples to six different to six different VOCs.

Table S1. Ag/NiO 0.5% response to six different VOCs.

Ag/NiO 0.5%	150 °C	200 °C	250 °C	300 °C	350 °C
Acetone	1.07	1.05	1.30	1.87	1.51
Ethanol	1.27	1.28	1.53	1.87	1.44
2-butanone	1.14	1.10	1.60	2.13	1.59
3-methyl-1-butanol	1.57	2.03	2.03	2.14	1.50
2-nonanone	1.08	1.18	1.32	1.20	1.08
m-xylene	1	1	1.17	1.71	1.73

Reference: Elaborated by the author.

Table S2. Ag/NiO 1% response to six different VOCs.

Ag/NiO 1%	150 °C	200 °C	250 °C	300 °C	350 °C
Acetone	1	1.05	1.08	1.02	1
Ethanol	1.08	1.07	1.08	1.03	1
2-butanone	1.06	1.02	1.11	1.04	1.02
3-methyl-1-butanol	1.22	1.16	1.22	1.08	1
2-nonanone	1.05	1.03	1.05	1	1
m-xylene	1.01	1.08	1.12	1.04	1

Reference: Elaborated by the author.

Table S3. Ag/NiO 2% response to six different VOCs.

Ag/NiO 2%	150 °C	200 °C	250 °C	300 °C	350 °C
Acetone	1.60	1.11	1.14	1.03	1
Ethanol	1.79	1.10	1.14	1.03	1
2-butanone	1.70	1.12	1.18	1.04	1
3-methyl-1-butanol	1,80	1.24	1.31	1.09	1
2-nonanone	1.08	1.05	1.05	1.02	1
m-xylene	1	1.18	1.17	1	1

Reference: Elaborated by the author.

Table S4. Ag/NiO 5% response to six different VOCs.

Ag/NiO 5%	150 °C	200 °C	250 °C	300 °C	350 °C
Acetone	1.24	1.46	1.29	1.09	1.02
Ethanol	1.82	1.56	1.47	1.08	1.02
2-butanone	1.49	1.40	1.41	1.11	1.02
3-methyl-1-butanol	2.20	2.59	1,95	1.17	1.03
2-nonanone	1.18	1.11	1.03	1	1
m-xylene	1.03	1.17	1.17	1.25	1.05

Reference: Elaborated by the author.